**Title**

Intravoxel incoherent motion (IVIM) histogram biomarkers for prediction of neoadjuvant treatment response in breast cancer patients.

**Permalink**

https://escholarship.org/uc/item/3gx6c3cp

**Authors**

Cho, Gene
Gennaro, Lucas
Sutton, Elizabeth
et al.

**Publication Date**

2017

**DOI**

10.1016/j.ejro.2017.07.002

Peer reviewed

# Intravoxel incoherent motion (IVIM) histogram biomarkers for prediction of neoadjuvant treatment response in breast cancer patients

Gene Y. Cho[a,b,c], Lucas Gennaro[a], Elizabeth J. Sutton[a], Emily C. Zabor[d], Zhigang Zhang[d], Dilip Giri[e], Linda Moy[b,c], Daniel K. Sodickson[b,c], Elizabeth A. Morris[a], Eric E. Sigmund[b,c,*,1], Sunitha B. Thakur[a,f,1]

[a] Department of Radiology, Memorial Sloan Kettering Cancer Center, New York, NY, 10065, USA
[b] Bernard and Irene Schwartz Center for Biomedical Imaging, Department of Radiology, New York School of Medicine, New York, NY, 10016, USA
[c] Center for Advanced Imaging Innovation and Research (CAI2R), New York University Langone Medical Center, New York, NY, 10016, USA
[d] Department of Epidemiology and Biostatistics, Memorial Sloan-Kettering Cancer Center, New York, NY, 10065, USA
[e] Department of Pathology, Memorial Sloan Kettering Cancer Center, New York, NY, 10065, USA
[f] Department of Medical Physics, Memorial Sloan Kettering Cancer Center, New York, NY, 10065, USA

## ARTICLE INFO

## ABSTRACT

*Objective:* To examine the prognostic capabilities of intravoxel incoherent motion (IVIM) metrics and their ability to predict response to neoadjuvant treatment (NAT). Additionally, to observe changes in IVIM metrics between pre- and post-treatment MRI.

*Methods:* This IRB-approved, HIPAA-compliant retrospective study observed 31 breast cancer patients (32 lesions). Patients underwent standard bilateral breast MRI along with diffusion-weighted imaging before and after NAT. Six patients underwent an additional IVIM-MRI scan 12–14 weeks after initial scan and 2 cycles of treatment. In addition to apparent diffusion coefficients (ADC) from monoexponential decay, IVIM mean values (tissue diffusivity $D_t$, perfusion fraction $f_p$, and pseudodiffusivity $D_p$) and histogram metrics were derived using a biexponential model. An additional filter identified voxels of highly vascular tumor tissue (VTT), excluding necrotic or normal tissue. Clinical data include histology of biopsy and clinical response to treatment through RECIST assessment. Comparisons of treatment response were made using Wilcoxon rank-sum tests.

*Results:* Average, kurtosis, and skewness of pseudodiffusion $D_p$ significantly differentiated RECIST responders from nonresponders. ADC and $D_t$ values generally increased (~70%) and VTT% values generally decreased (~20%) post-treatment.

*Conclusion:* $D_p$ metrics showed prognostic capabilities; slow and heterogeneous pseudodiffusion offer poor prognosis. Baseline ADC/$D_t$ parameters were not significant predictors of response. This work suggests that IVIM mean values and heterogeneity metrics may have prognostic value in the setting of breast cancer NAT.

## 1. Introduction

Diffusion weighted imaging (DWI) can be useful in characterizing cancerous tissue heterogeneity, motivating its broad adoption in oncologic management. While random water diffusion is found in all fluids, biological tissues can contribute to both active transport or pseudodiffusion effects to which DWI is sensitive; this is especially true with highly vascularized cancer tissue. Through DWI, biomarkers have been developed that are sensitive to microvascular flow via intravoxel incoherent motion (IVIM) analysis [1].

Using IVIM, one can quantify the tumor hypervascularity and hypercellularity, which has been shown in a range of breast cancer studies [2–8]. Furthermore, histogram analysis of the spatial distribution of IVIM parameters can provide additional markers (e.g. skewness and kurtosis) for characterization of the heterogeneity of the tumor microenvironment [2–12].

While IVIM metrics can distinguish between benign and malignant breast lesions [2,3,5,11,13], there is also interest in determining whether these IVIM metrics can predict treatment response or segment patient populations based on degree of response to treatment. Neoadjuvant treatment (NAT), which has traditionally been used for locally advanced breast cancer [14], is increasingly used in operable breast

cancer because it can be as effective as adjuvant chemotherapy. Additionally, it allows breast conservation in women who historically required mastectomy. Moreover, response to NAT has been shown to vary with breast cancer molecular subtype with the best possible outcome, pathological complete response (pCR), being associated with improved disease free survival [14,15]. However, pCR rates after NAT are around 20–30% [15,16], and broken down by molecular subtype, they range from less than 10% for Luminal A to 50–60% for Her2-positive, ER negative subtypes [17,18]. Accordingly, NAT can be used as an *in vivo* test for chemo-sensitivity, thereby providing prognostic information with respect to long term response to treatment [16]. Therefore, there is motivation to better understand, segment, and develop prognoses for the patient population that does not report pCR.

A key advantage of an imaging marker of response to NAT is an early stratification between patients who have pCR, those who show response to NAT, and those who do not. Such a biomarker will provide utility in treatment planning as clinicians can assess the effectiveness of treatments early to avoid debilitating side effects, minimize treatment costs, and expedite alternative treatment protocols to increase overall survival. At present, pre- and post-NAT contrast-enhanced MRI (CE-MRI) are commonly used to evaluate response of a tumor to NAT [19]. However, there are limitations to CE-MRI as well as risks in using contrast agents for the minority of patients with impaired kidney function. Therefore, finding an alternative non-contrast imaging tool capable of predicting treatment response in the NAT setting is highly valued. Finally, beyond the highly desirable outcome of pCR in NAT, quantitative imaging can provide guidance on improved operability through tumor size reduction. Even when pCR is not achieved in the pre-surgical period, tumors can be dramatically downsized for excision and adjuvant treatment. The ability of quantitative imaging, such as IVIM, to stratify these partial responders is an area of great potential.

Conventional diffusion weighted imaging quantified by apparent diffusion coefficient (ADC) has an increasing track record in prognostic applications with a growing literature in the case of breast cancer [20–22]. The IVIM method has recently been applied to neoadjuvant response prediction in breast cancer studies after therapy [10,23], considering mean values of IVIM metrics. To more extensively explore the prognostic utility of IVIM, in this study, we examine breast cancer patients using pre- and post-treatment imaging and compare the metrics from IVIM histogram analysis with treatment response.

## 2. Methods

### 2.1. Patients

This IRB approved, HIPAA-compliant retrospective study observed 31 breast cancer patients with 32 lesions (31 invasive ductal carcinoma and 1 invasive lobular carcinoma). All patients underwent two sets of MRI scans during April 2011 to March 2013 ('pre-treatment scans' and 'post-treatment scans') accompanied by dose-dense adjuvant doxorubicin-based treatments (N = 24), taxol-based treatments (N = 9), and docetaxel-based treatments (N = 3). All patients had their first treatment within 30 days of their first MRI exam. Patients were diagnosed with breast cancer through stereotactic, US, or MRI core biopsy. Table 1 shows patients' lesion characteristics and scanner magnetic field values. Final histopathology diagnosis was confirmed through histology, surgery, and clinical follow-up. Additionally, 6 of these patients underwent an extended post-treatment MRI scan with a multi b value diffusion-weighted imaging (DWI) approximately 16 weeks after the initiation of therapy ('post-treatment IVIM scans').

### 2.2. MRI scans

All patients underwent two standard bilateral breast MRI (pre-/post-treatment) using contrast enhancement in a full body 1.5 or 3T MRI scanner system (Discovery MR450/750; GE Healthcare, Waukesha, WI)

**Table 1**
Patient Lesion Characteristics. Numbers reported are N (%)[a].

| | All patients (N = 32) | Patients with 'post-treatment IVIM scans' (N = 6) |
|---|---|---|
| **Type** | | |
| IDC | 31 (96.9) | 6 (100) |
| ILC | 1 (3.1) | 0 (0) |
| **Histology Grade** | | |
| 2 | 2 (6.2) | 0 (0) |
| 3 | 28 (87.5) | 6 (100) |
| NA | 2 (6.2) | 0 (0) |
| **Nuclear Grade** | | |
| 2 | 8 (25) | 2 (33.3) |
| 3 | 18 (56.2) | 4 (66.7) |
| NA | 6 (18.8) | 0 (0) |
| **Subtypes** | | |
| HER2+ | 4 (12.5) | 1 (16.7) |
| Luminal-A | 12 (37.5) | 1 (16.7) |
| Luminal-B | 8 (25) | 3 (50) |
| Triple Negative | 8 (25) | 1 (16.7) |
| **LVI** | | |
| Negative | 7 (21.9) | 0 (0) |
| Positive | 24 (75) | 6 (100) |
| NA | 1 (3.1) | 0 (0) |
| **Pathological Complete Response** | | |
| pCR | 4 (14.5) | 0 (0) |
| No pCR | 28 (87.5) | 6 (100) |
| **RECIST** | | |
| CR or PR | 27 (84.4) | 5 (83.3) |
| PD or SD | 5 (15.6) | 1 (16.7) |
| **Magnetic Field** | | |
| 1.5T | 7 (21.9) | 2 (33.3) |
| 3T | 25 (78.1) | 4 (66.7) |

[a] Abbreviations: IDC − Invasive Ductal Carcinoma, ILC − Invasive Lobular Carcinoma, SD/PD − Stable/Progressive Disease, PR/CR − Partial/Complete Response, LVI − Lymphovascular invasion, NA − Not Available.

with either an 8 (3T) or 16 channel (1.5T) breast coil (Sentinelle Medical, Toronto, Canada), MR examinations included fat-suppressed T1- and T2-weighted imaging before and at three time points after the administration of intravenous contrast. All patients (n = 31) also underwent a multi b value DWI protocol ('pre-treatment IVIM scans') consisted of a single shot spin echo EPI sequence (TR/TE = 4000/85.3 ms; 4 averages; FOV = 28 × 28 to 36 × 36 cm$^2$; slice thickness: 4–5 mm; acquired matrix: 128 × 128, interpolated to 256 × 256; 19–35 slices; and 10 b values, with b = 0, 30, 60, 90, 120, 250, 400, 600, 800, 1000 s/mm$^2$), while 6 of 31 patients underwent a second multi b value DWI protocol ('post-treatment IVIM scans').

### 2.3. Image analysis

A breast radiologist (L.G..) identified lesions on anatomical post contrast T1 weighted images based on hyperintense signals from axial images, then region of interests (ROIs) were drawn on the DWI by another operator (G.Y.C.). Quantitative analysis of DWI was performed with custom analysis code (Igor Pro 6, Wavemetrics, Inc., Portland, USA) [2]. Images were first analyzed voxel-by-voxel using a mono-exponential decay model with all b values to produce apparent diffusion coefficient (ADC) maps for all slices:

$$M / M_0 = e^{-b \cdot ADC} \tag{1}$$

ADC maps, DWI images, and post-contrast T1-weighted images guided lesion segmentation for quantitative IVIM. ROIs were drawn on the largest single slice tumor area and analyzed for all b values. The cross-sectional area of the lesion as measured on DWI was recorded for each patient.

To distinguish signal attenuation due to microcirculation-induced spin dephasing from diffusion induced signal attenuation, a biexponential analysis was used to quantify microvascular and tissue structural properties. The signal decay curve was measured as a function of increasing b value and fitted to a biexponential equation:

$$M \quad / M_0 = f_p \cdot e^{-b \cdot D_p} + (1 - f_p) \cdot e^{-b \cdot D_t} \tag{2}$$

where $M_0$ is total reference magnetization, $f_p$ is perfusion fraction, $D_p$ is pseudo-diffusivity, and $D_t$ is tissue diffusivity. For all analyses, a "segmented" approach was employed by fitting the higher b value region (b > 200 s/mm$^2$) to calculate IVIM parameters, $f_p$ and $D_t$, and then extracting $D_p$ from a constrained fit to the entire b value set [2].

In addition, implementation of a vascular tumor tissue (VTT) filter was used for parametric map analysis [24]. Since voxel-wise IVIM analysis allows the delineation of viable tumor tissue within a typically heterogeneous texture of cellularity, necrosis, and normal tissue, one can apply a filter (VTT filter) that selectively chooses voxels that are most critical or relevant, i.e. highly vascular tissue that signifies the most aggressive regions of the cancer. This filter, based on the Aikake information criterion to test applicability of each voxel's biexponential fit [24] provided the number of voxels of vascular tumor tissue, as a fraction of total lesion voxels. Finally, histogram analysis on all lesion voxels was performed to quantify tumor heterogeneity [2] with mean, maximum, minimum and heterogeneity metrics (standard deviation, skewness and kurtosis). The full workflow employed was described previously [2].

### 2.4. Clinical data

Data collected include histology of biopsy and surgical specimens to determine pathological complete response, (pCR). Another method of observing response was the RECIST criteria, where tumor size reduction was measured using pre- and post-treatment post-contrast T1 images [Complete response (CR) − disappearance of target lesion; partial response (PR) − at least 30% decrease in the sum of diameters of the target lesion, taking as reference the baseline sum of diameters; progressive disease (PD) − at least 20% increase in the sum of diameters of the target lesion; and stable disease (SD) − neither sufficient shrinkage for PR or sufficient enlargement for PD] [25]. One patient was excluded for lack of response data while 1 smaller lesion (< 2 cm) was excluded. Table 1 shows patients' prognostic factor data. IVIM biomarkers were tested for prognosis of response as defined by RECIST criteria.

### 2.5. Statistical analysis

One subject contributed two observations due to bilateral breast cancer; all other subjects contributed only one observation. Differences in IVIM parameters by treatment response were tested using the Wilcoxon rank-sum test. Adjustment for multiple comparisons was made using the false discovery rate (FDR) method, which controls the expected proportion of null hypotheses that are incorrectly rejected. A p-value < 0.05 was considered statistically significant. P-values are shown both before and after adjustment for multiple comparisons. Statistical analyses were conducted in R software version 3.1.1 (R Core Development Team, Vienna, Austria).

## 3. Results

### 3.1. Patients

Mean age of all patients was 47.40 ± 8.84 years (50.18 ± 10.51 years for responders, 46.26 ± 11.66 years for nonresponders) with a range of 28–66 years. All analyzed lesions had a diameter that was greater than 2 cm on contrast-enhanced imaging and median (minimum, maximum) ROI size from DWI segmentation was

13.84 (3.43, 44.45) cm$^2$. Additionally, all patients with pCR were considered responders according to RECIST criteria (all patients with RECIST criteria of CR were determined to be pCR); all other patients with other RECIST criteria were reported to have no pCR. A total of twenty four patients underwent a 3T MRI pre-treatment scan, while seven patients underwent a 1.5T MRI pre-treatment scan. Among the six patients who had both a pre- and post-treatment scan, two patients underwent a 1.5T MRI pre-treatment then a 3T MRI post-treatment scan while one patient had a pre-treatment 3T scan and a 1.5T post-treatment scan. The other three patients all received 3T MRI pre-/post-treatment scans.

For the pre-treatment data, the median (minimum, maximum) value of average ADC found for all lesions was 1.10 (0.56, 2.18) μm$^2$/ms, with 1.11 (0.56, 2.18) μm$^2$/ms for all 3T results and 1.10 (0.76, 2.17) μm$^2$/ms for all 1.5T results. The median (minimum, maximum) values of average $D_t$, $f_p$, and $D_p$ found for all lesions were 1.02 (0.55, 2.16) μm$^2$/ms, 8.8 (4.8, 19.3) %, and 25.05 (15.99, 37.14) μm$^2$/ms, respectively. The median (minimum, maximum) values for IVIM metrics stratified by field strength were $D_t$ = 1.02 (0.55, 2.15) μm$^2$/ms, $f_p$ = 8.9 (4.8, 15.8) %, and $D_p$ = 25.52 (15.99, 37.14) μm$^2$/ms for 3T, and $D_t$ = 1.04 (0.71, 2.16) μm$^2$/ms, $f_p$ = 8.7 (5.1, 19.3) %, and $D_p$ = 22.04 (20.11, 35.73) μm$^2$/ms for 1.5T. The values at different field strengths were similar (Fig. 1), and no significant differences were found between metrics obtained from different magnetic field strengths.

### 3.2. Comparison of pre-treatment IVIM with clinical response to treatment

The median (minimum, maximum) values of average ADC for RECIST nonresponders versus responders to treatment was 1.14 (1.11, 1.28) μm$^2$/ms versus 1.07 (0.56, 2.18) μm$^2$/ms. For median (minimum, maximum) values of average $D_t$, $f_p$, and $D_p$, the average values were 1.05 (0.96, 1.21) μm$^2$/ms, 11.7 (5.2, 14.2)%, and 17.16 (16.9, 25.79) μm$^2$/ms for nonresponders, while for responders they were 0.99 (0.55, 2.16) μm$^2$/ms, 8.7 (4.8, 19.3)%, and 25.54 (15.99, 37.14) μm$^2$/ms. The pre-treatment median (minimum, maximum) lesion size on DWI was 13.80 (3.43, 37.0) cm$^2$ for RECIST responders and 23.98 (8.73, 44.45) cm$^2$ for RECIST nonresponders; these values were not found to be significantly different. Table 2 shows ADC and IVIM average and histogram metric median values as well as VTT% and lesion size as a function of response to treatment. Average, skewness, and kurtosis of the $D_p$ parameters significantly differentiated between RECIST responders and nonresponders to treatment before adjustment for multiple comparisons (Fig. 1). Furthermore, VTT% nearly significantly differentiated (p = 0.52) between RECIST responders and nonresponders (median values − 30.0% versus 40.7%, respectively) prior to adjustment for multiple comparisons. These significant findings also held true when selecting for patients who underwent 3T MRI scans. Once the results were adjusted using multiple comparisons, none of the findings were considered significant though $D_p$ skewness merits further study. In addition, ADC and $D_t$ had lower values for responders to treatment, but were not found to be significant response predictors.

### 3.3. Comparison of pre- and post-treatment IVIM

Next, we observe that the IVIM parameters changed when comparing between pre- and post-treatment MRI scans in six patients. Fig. 2 shows the parametric maps of pre- and post-treatment of a RECIST responding patient with invasive ductal carcinoma (IDC), while Fig. 3 shows the pre- and post-treatment maps of a RECIST nonresponding patient with IDC. Lesion size reduction is clearly observable in the responding patient while ADC and IVIM parameters also show noticeable differences with treatment (Fig. 2). ADC and $D_t$ values show increases while $f_p$ and $D_p$ are more heterogeneous in the post-treatment maps. In the nonresponding patient, the change in lesion size is not noticeable; however, some increased heterogeneity is seen in the post-treatment maps (Fig. 3). At the group level, ADC and $D_t$ values increased
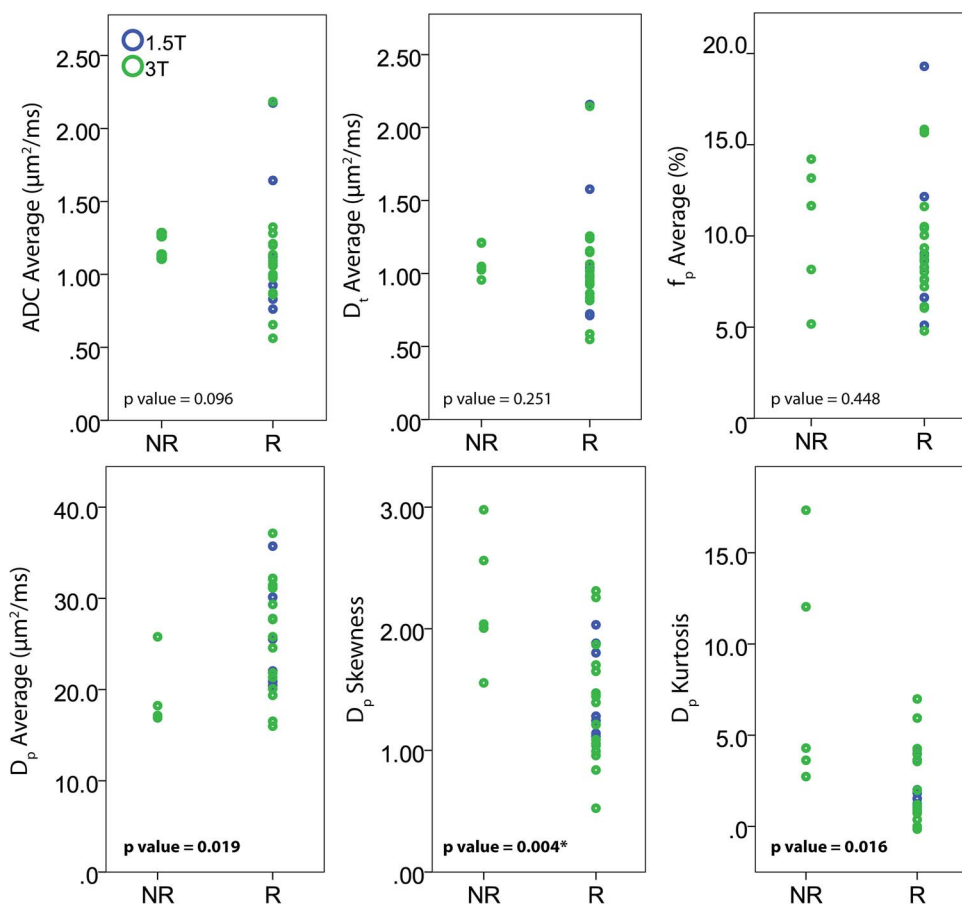
**Fig. 1.** IVIM metrics in breast cancer patients stratified by field strength and RECIST response group. Unadjusted p-values for comparison of responders (R) to non-responders (NR) are shown.

(+70.4% and +74.1%, respectively) and VTT% values decreased post-treatment (−21.0%). Average tumor size reduction was −40.2%. Five dual scanned patients were responders while one patient was a non-responder. Fig. 4 shows IVIM, VTT%, and lesion size values for each patient before and after treatment. $D_p$ values generally decreased post-treatment (Fig. 4).

## 4. Discussion

Comparisons of IVIM metrics with clinical response results showed

**Table 2**
Pre-treatment IVIM average and histogram metric median (min, max) values between RECIST responders and non-responders. Raw and adjusted p-values for Wilcoxon rank-sum test comparing responders to non-responders are given, with significant group differences in bold.

| | | Overall (N = 32) | Responders (N = 27) | Nonresponders (N = 5) | p | adj. p |
|---|---|---|---|---|---|---|
| ADC (μm²/ms) | Maximum | 2.16 (1.15, 3.00) | 2.20 (1.15, 3.00) | 2.13 (1.65, 2.93) | 0.938 | 0.938 |
| | Minimum | 0.49 (0.01, 1.34) | 0.48 (0.01, 1.34) | 0.54 (0.05, 0.67) | 0.697 | 0.914 |
| | Kurtosis | 0.98 (−1.17, 4.90) | 0.97 (−1.17, 4.90) | 1.07 (−0.30, 4.83) | 0.815 | 0.938 |
| | Skewness | 0.73 (−1.33, 2.05) | 0.78 (−1.33, 2.05) | 0.21 (−0.72, 1.80) | 0.337 | 0.914 |
| | Average | 1.10 (0.56, 2.18) | 1.07 (0.56, 2.18) | 1.14 (1.11, 1.28) | 0.103 | 0.453 |
| | St. Dev. | 0.30 (0.10, 0.61) | 0.30 (0.10, 0.61) | 0.31 (0.14, 0.37) | 0.856 | 0.938 |
| $D_t$ (μm²/ms) | Maximum | 1.91 (1.12, 2.89) | 1.90 (1.12, 2.89) | 1.96 (1.64, 2.35) | 0.452 | 0.914 |
| | Minimum | 0.42 (0.01, 1.37) | 0.4 (0.01, 1.37) | 0.48 (0.05, 0.62) | 0.938 | 0.938 |
| | Kurtosis | 0.76 (−1.08, 4.52) | 0.74 (−1.08, 4.43) | 1.01 (−0.42, 4.52) | 0.736 | 0.914 |
| | Skewness | 0.64 (−1.23, 1.94) | 0.78 (−1.23, 1.94) | 0.27 (−0.61, 1.36) | 0.659 | 0.914 |
| | Average | 1.02 (0.55, 2.16) | 0.99 (0.55, 2.16) | 1.05 (0.96, 1.21) | 0.287 | 0.914 |
| | St. Dev. | 0.26 (0.08, 0.59) | 0.25 (0.08, 0.59) | 0.26 (0.14, 0.35) | 0.938 | 0.938 |
| $f_p$ | Maximum (%) | 29.8 (12.2, 83.1) | 29.6 (12.2, 83.1) | 32.5 (15.9, 69.2) | 0.622 | 0.914 |
| | Kurtosis | 0.72 (−0.85, 23.56) | 0.62 (−0.85, 23.56) | 3.37 (−0.85, 5.61) | 0.697 | 0.914 |
| | Skewness | 0.96 (0.04, 4.54) | 0.96 (0.27, 4.54) | 1.73 (0.04, 1.88) | 0.622 | 0.914 |
| | Average (%) | 8.8 (4.8, 19.3) | 8.7 (4.8, 19.3) | 11.7 (5.2, 14.2) | 0.483 | 0.914 |
| | St. Dev. (%) | 5.6 (2.5, 17.0) | 5.2 (2.5, 17.0) | 7.2 (3.2, 11.4) | 0.586 | 0.914 |
| $D_p$ (μm²/ms) | Maximum | 96.43 (71.36, 99.94) | 96.42 (71.36, 99.8) | 97.42 (80.7, 99.94) | 0.659 | 0.914 |
| | Minimum | 0.66 (0.01, 3.07) | 0.80 (0.03, 3.07) | 0.27 (0.01, 2.16) | 0.186 | 0.690 |
| | Kurtosis | 2.37 (−0.15, 17.33) | 1.98 (−0.15, 6.99) | 4.29 (2.73, 17.33) | **0.021** | 0.181 |
| | Skewness | 1.42 (0.52, 2.98) | 1.24 (0.52, 2.31) | 2.04 (1.55, 2.98) | **0.005** | 0.143 |
| | Average | 25.05 (15.99, 37.14) | 25.54 (15.99, 37.14) | 17.16 (16.9, 25.79) | **0.018** | 0.181 |
| | St. Dev. | 17.04 (7.49, 23.44) | 16.82 (14.38, 23.44) | 19.24 (7.49, 19.71) | 0.622 | 0.914 |
| VTT% | | 35.0 (10.3, 72) | 30.0 (10.3, 64.8) | 40.7 (38.4, 72) | 0.052 | 0.335 |
| Lesion Size (cm²) | | 13.84 (3.43, 44.45) | 13.80 (3.43, 37.00) | 23.98 (8.73, 44.45) | 0.248 | 0.607 |

**Fig. 2.** Pre- and post-treatment IVIM maps for a RECIST responding patient (no pCR) with invasive ductal carcinoma.
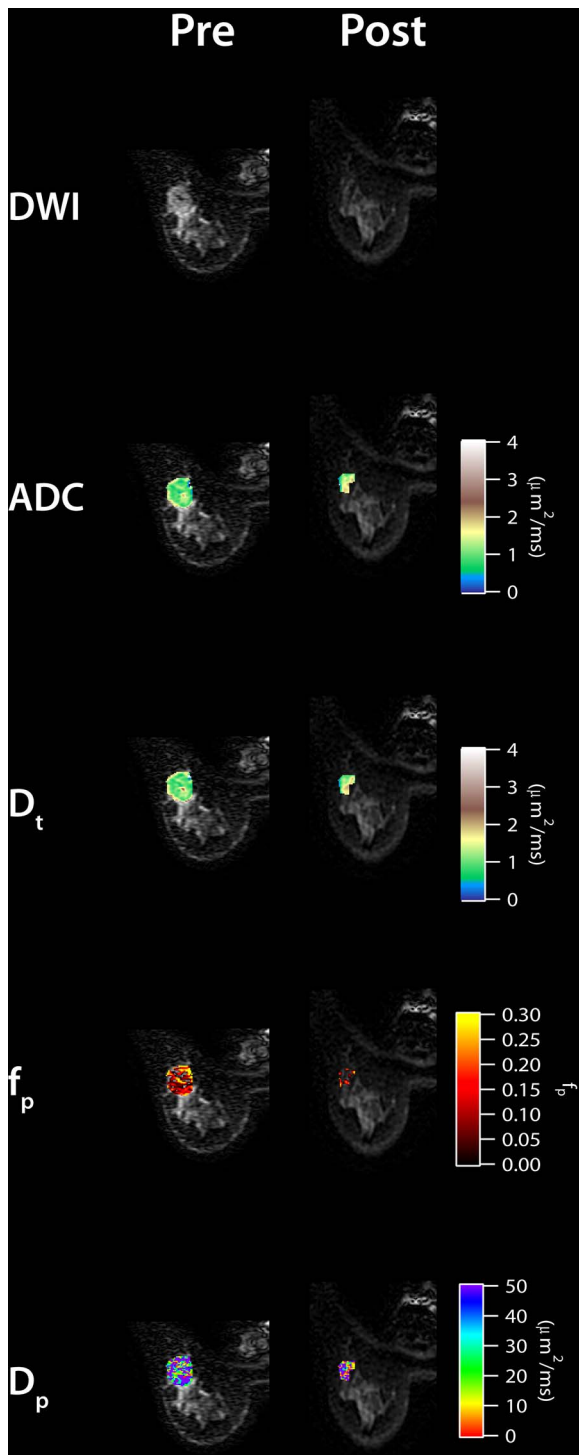


**Fig. 3.** Pre- and post-treatment IVIM maps for a RECIST nonresponding patient with invasive ductal carcinoma.

that certain IVIM parameters were able to differentiate between RECIST responders and nonresponders. Among baseline measurements, $D_p$ and VTT% were the most prognostic as high vascularity with slow and heterogeneous pseudodiffusion offering poor prognosis; in a related sense, decreases in $D_p$ occurred in all dual-scanned responders. Moreover, the heterogeneity metrics of $D_p$ showed the most interesting results and demonstrated the utility of using advanced metrics within IVIM analysis. The significant findings from histogram analysis show the potential to identify differences in tumor heterogeneity between responders and nonresponders. These $D_p$ and VTT% results illustrate
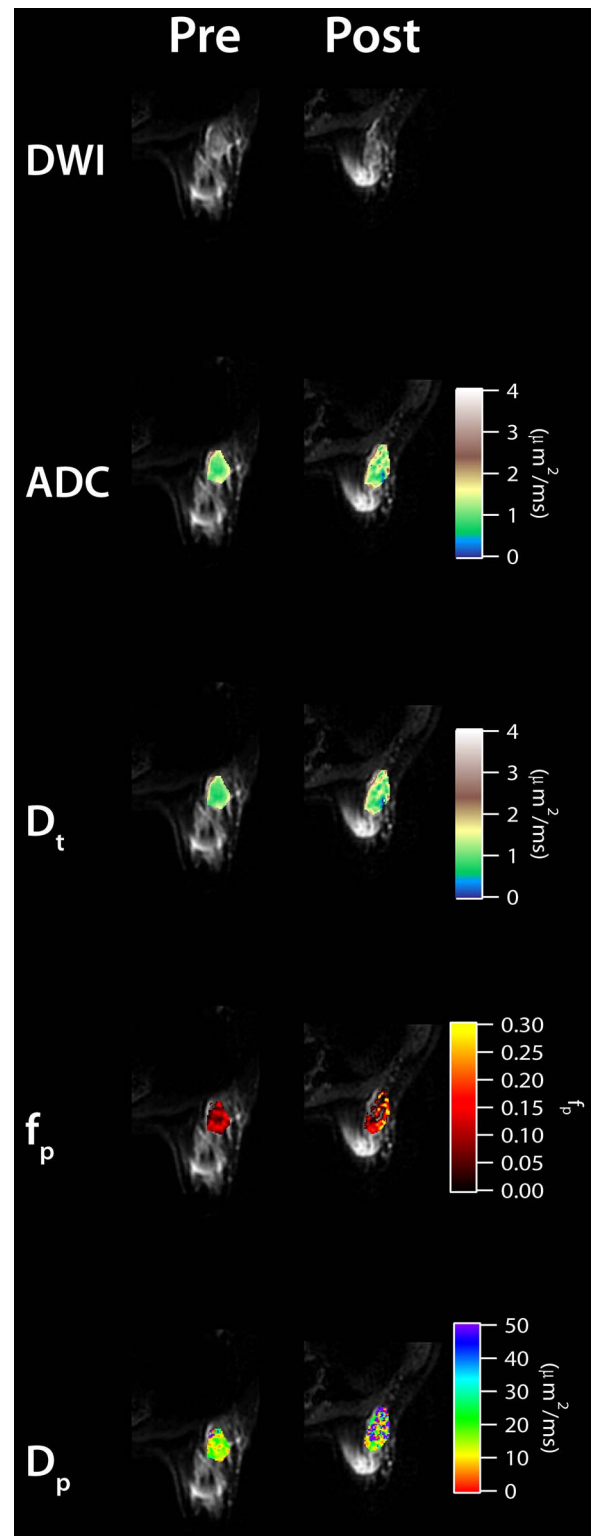
that the vascular entities from lesions may be most useful at predicting response to NAT, and characterization of heterogeneous distribution of blood volume may be an ideal predictor of response. Some recent cancer studies have noticed IVIM differences when comparing between responders and nonresponders [10,26], showing that vascular, along with cellular, IVIM parameters can be predictive of response [10]. These observations are similar to the results found in this study. Beyond
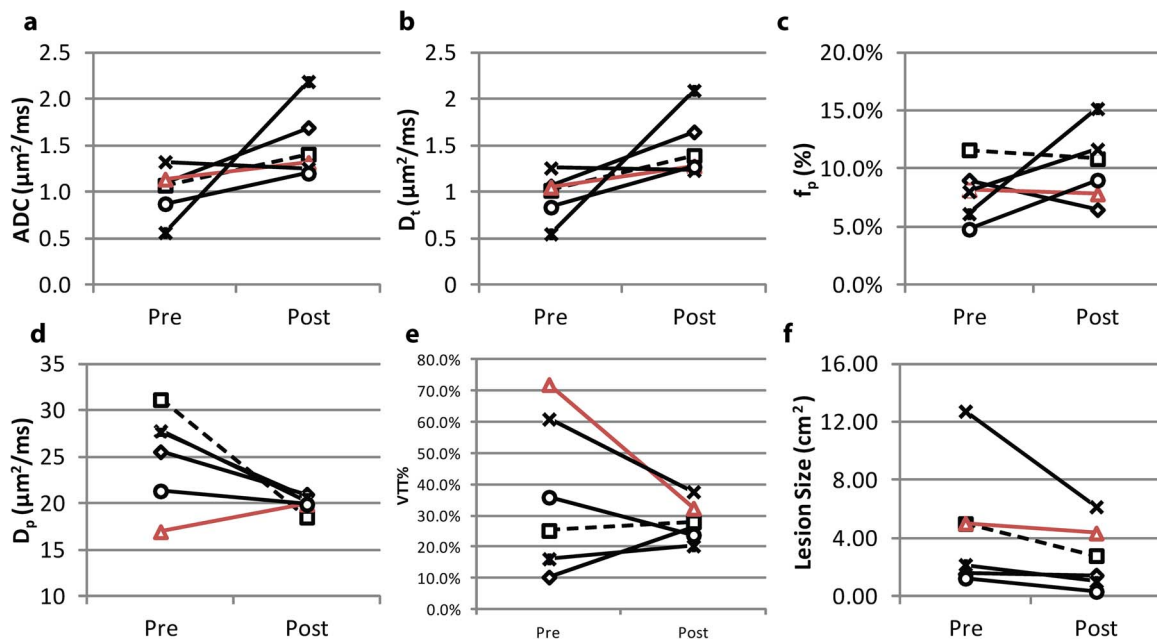
**Fig. 4.** IVIM metrics (a-d), VTT% (e), and pre-/post-treatment size (cm$^2$) (f) for the six patients with pre-/post-treatment scans. Red line (triangle symbol) indicates the patient who was labeled as a RECIST nonresponder (Fig. 3). The RECIST responding patient from Fig. 2 is indicated by the dashed line. (For interpretation of the references to colour in this figure legend, the reader is referred to the web version of this article.)

this trend, the expansion of IVIM analysis using histograms in this study can lend further support to better characterize the lesion vascularity.

It should be noted that breast diffusion MRI studies in the neoadjuvant setting used different ways to define response: four studies used pCR [10,23,27,28] and three studies used RECIST [20–22]. In our study, we focused on RECIST to illustrate the potential of IVIM-MRI in predicting improved surgical operability of breast lesions. However, RECIST and pCR criteria did correlate in terms of those exhibiting complete response. Therefore, there remains strong motivation for having markers of response to NAT to improve treatment planning for surgery, increase operability, avoid debilitating side effects and expedite alternative treatments.

The IVIM parameters changes in patients who underwent pre- and post-treatment MRI scans may be due to the effects of doxorubicin, herceptin, or taxol-based NAT, which is known to change both the vascularity and cellularity of tumors based on their anti-angiogenic and cytotoxic effects [21,29]. While the sample size (six patients), protocol variations (e.g. type of treatment, scan time after treatment, field strength, etc.), and infeasibility of inter-scan image registration (due to large morphologic changes) limited strong conclusions, general trends could still be observed between pre- and post-treatment scans.

Unlike previous studies [21], baseline values of ADC or $D_t$ were not predictive of response in our cohort, although early increases in ADC and $D_t$ values were observed to be largest in dual-scanned responders, suggesting a decline in cellularity. Baseline ADC trended towards significance, but in our cohort, this trend seems to have been dominated by vascular rather than cellular component as $D_t$ showed no trends. Additionally, Che et al. [10] found baseline $f_p$, mid-treatment $f_p$ and $D_t$, and pre/post changes to $D_t$ and $f_p$ to predict response, while Bedair et al. [23] found baseline ADC, $D_t$, and stretched exponential distributed diffusion coefficient (DDC), as well as pre/post changes in ADC, DDC and $f_p$ to predict response. The lack of uniformity of protocol and patients in this study may have contributed to our different findings. However, this present study highlights the fact that both mean values and heterogeneity metrics from microvascular DWI parameters can have useful prognostic value in the setting of breast cancer.

This study was limited by several factors. First, patient population size was small, limiting statistical power and precluding multivariable analysis. Neither field strength nor neoadjuvant treatment protocol was controlled for in the enrollment paradigm; however, our initial observations showed very little bias based on these differences in field strength and studies have shown that protocols can be used to diminish the variations caused by differing field strength [29]. Future work will explore a standardized, uniform IVIM approach in the setting of breast cancer for more robust results. All of the significant findings did not persist when using multiple group comparison corrections; however, some findings, i.e. $D_p$ skewness, showed results that are worthy of further study. Moreover, multiple comparison correction methods may often be too conservative for empirical research, especially in our case, when statistical tests are only performed where there is strong knowledge or understanding for expecting a certain result. While these corrections control for false positives, they do so at the potential expense of many more false negatives. Finally, there have been some concerns in regards to the low repeatability/reproducibility of certain IVIM parameters ($f_p$, $D_p$) in some contexts [30] and we have not considered this aspect in this study.

In conclusion, this work represents a step forward in understanding the utility of diffusion MRI and IVIM. These tools can provide useful clinical, non-invasive biomarkers during cancer diagnosis and treatment. We demonstrate that several IVIM biomarkers show potential as predictors of treatment response to NAT. We also illustrate spatially dependent physiological changes that are observed after treatment. Further studies should be conducted to solidify the prognostic value of the IVIM biomarkers in longitudinal breast cancer studies for treatment and outcome monitoring.

**Conflicts of interest**

The authors declare that there no conflict of interest.

**Acknowledgements**

# References

[1] D. Le Bihan, E. Breton, D. Lallemand, M.L. Aubin, J. Vignaud, M. Laval-Jeantet, Separation of diffusion and perfusion in intravoxel incoherent motion MR imaging, Radiology 168 (2) (1988) 497–505.

[2] G.Y. Cho, L. Moy, S.G. Kim, S.H. Baete, M. Moccaldi, J.S. Babb, D.K. Sodickson, E.E. Sigmund, Evaluation of breast cancer using intravoxel incoherent motion (IVIM) histogram analysis: comparison with malignant status, histological subtype, and molecular prognostic factors, Eur. Radiol. 26 (8) (2016) 2547–2558.

[3] M. Iima, K. Yano, M. Kataoka, M. Umehana, K. Murata, S. Kanao, K. Togashi, D. Le Bihan, Quantitative non-Gaussian diffusion and intravoxel incoherent motion magnetic resonance imaging: differentiation of malignant and benign breast lesions, Invest. Radiol. 50 (4) (2015) 205–211.

[4] S. Suo, N. Lin, H. Wang, L. Zhang, R. Wang, S. Zhang, J. Hua, J. Xu, Intravoxel incoherent motion diffusion-weighted MR imaging of breast cancer at 3.0 tesla: comparison of different curve-fitting methods, J. Magn. Reson. Imaging: JMRI 42 (2) (2015) 362–370.

[5] L. Bokacheva, J.B. Kaplan, D.D. Giri, S. Patil, M. Gnanasigamani, C.G. Nyman, J.O. Deasy, E.A. Morris, S.B. Thakur, Intravoxel incoherent motion diffusion-weighted MRI at 3.0 T differentiates malignant breast lesions from benign lesions and breast parenchyma, J. Magn. Reson. Imaging: JMRI 40 (4) (2014) 813–823.

[6] E.E. Sigmund, G.Y. Cho, S. Kim, M. Finn, M. Moccaldi, J.H. Jensen, D.K. Sodickson, J.D. Goldberg, S. Formenti, L. Moy, Intravoxel incoherent motion imaging of tumor microenvironment in locally advanced breast cancer, Magn. Reson. Med. 65 (5) (2011) 1437–1447.

[7] H. Dijkstra, M.D. Dorrius, M. Wielema, K. Jaspers, R.M. Pijnappel, M. Oudkerk, P.E. Sijens, Semi-automated quantitative intravoxel incoherent motion analysis and its implementation in breast diffusion-weighted imaging, J. Magn. Reson. Imaging: JMRI 43 (5) (2016) 1122–1131.

[8] Y.J. Lee, S.H. Kim, B.J. Kang, Y.J. Kang, H. Yoo, J. Yoo, J. Lee, Y.H. Son, R. Grimm, Intravoxel incoherent motion (IVIM)-derived parameters in diffusion-weighted MRI: Associations with prognostic factors in invasive ductal carcinoma, J. Magn. Reson. Imaging: JMRI 45 (5) (2017) 1394–1406.

[9] R. Panek, M. Borri, M. Orton, E. O'Flynn, V. Morgan, S.L. Giles, N. deSouza, M.O. Leach, M.A. Schmidt, Evaluation of diffusion models in breast cancer, Med. Phys. 42 (8) (2015) 4833–4839.

[10] S. Che, X. Zhao, Y. Ou, J. Li, M. Wang, B. Wu, C. Zhou, Role of the intravoxel incoherent motion diffusion weighted imaging in the pre-treatment prediction and early response monitoring to neoadjuvant chemotherapy in locally advanced breast cancer, Medicine 95 (4) (2016) e2420.

[11] C. Liu, K. Wang, Q. Chan, Z. Liu, J. Zhang, H. He, S. Zhang, C. Liang, Intravoxel incoherent motion MR imaging for breast lesions: comparison and correlation with pharmacokinetic evaluation from dynamic contrast-enhanced MR imaging, Eur. Radiol. 26 (11) (2016) 3888–3898.

[12] D. Ma, F. Lu, X. Zou, H. Zhang, Y. Li, L. Zhang, L. Chen, D. Qin, B. Wang, Intravoxel incoherent motion diffusion-weighted imaging as an adjunct to dynamic contrast-enhanced MRI to improve accuracy of the differential diagnosis of benign and malignant breast lesions, Magn. Reson. Imaging 36 (2017) 175–179.

[13] Q. Wang, Y. Guo, J. Zhang, Z. Wang, M. Huang, Y. Zhang, Contribution of IVIM to conventional dynamic contrast-enhanced and diffusion-weighted MRI in differentiating benign from malignant Breast masses, Breast Care (Basel, Switzerland 11 (4) (2016) 254–258.

[14] A.M. Thompson, S.L. Moulder-Thompson, Neoadjuvant treatment of breast cancer, Ann. Oncol. 23 (Suppl 10) (2012) x231–x236.

[15] M. Colleoni, A. Goldhirsch, Neoadjuvant chemotherapy for breast cancer: any progress? Lancet Oncol. 15 (2) (2014) 131–132.

[16] M. Kaufmann, G. von Minckwitz, E.P. Mamounas, D. Cameron, L.A. Carey, M. Cristofanilli, C. Denkert, W. Eiermann, M. Gnant, J.R. Harris, T. Karn, C. Liedtke, D. Mauri, R. Rouzier, E. Ruckhaeberle, V. Semiglazov, W.F. Symmans, A. Tutt, L. Pusztai, Recommendations from an international consensus conference on the current status and future of neoadjuvant systemic therapy in primary breast cancer, Ann. Surg. Oncol. 19 (5) (2012) 1508–1516.

[17] P. Cortazar, L. Zhang, M. Untch, K. Mehta, J.P. Costantino, N. Wolmark, H. Bonnefoi, D. Cameron, L. Gianni, P. Valagussa, S.M. Swain, T. Prowell, S. Loibl, D.L. Wickerham, J. Bogaerts, J. Baselga, C. Perou, G. Blumenthal, J. Blohmer, E.P. Mamounas, J. Bergh, V. Semiglazov, R. Justice, H. Eidtmann, S. Paik, M. Piccart, R. Sridhara, P.A. Fasching, L. Slaets, S. Tang, B. Gerber, C.E. Geyer Jr., R. Pazdur, N. Ditsch, P. Rastogi, W. Eiermann, G. von Minckwitz, Pathological complete response and long-term clinical benefit in breast cancer: the CTNeoBC pooled analysis, Lancet 384 (9938) (2014) 164–172.

[18] G. von Minckwitz, M. Untch, J.U. Blohmer, S.D. Costa, H. Eidtmann, P.A. Fasching, B. Gerber, W. Eiermann, J. Hilfrich, J. Huober, C. Jackisch, M. Kaufmann, G.E. Konecny, C. Denkert, V. Nekljudova, K. Mehta, S. Loibl, Definition and impact of pathologic complete response on prognosis after neoadjuvant chemotherapy in various intrinsic breast cancer subtypes, J. Clin. Oncol. 30 (15) (2012) 1796–1804.

[19] M.B. Lobbes, R. Prevos, M. Smidt, V.C. Tjan-Heijnen, M. van Goethem, R. Schipper, R.G. Beets-Tan, J.E. Wildberger, The role of magnetic resonance imaging in assessing residual disease and pathologic complete response in breast cancer patients receiving neoadjuvant chemotherapy: a systematic review, Insights Imaging 4 (2) (2013) 163–175.

[20] C.J. Galban, B. Ma, D. Malyarenko, M.D. Pickles, K. Heist, N.L. Henry, A.F. Schott, C.H. Neal, N.M. Hylton, A. Rehemtulla, T.D. Johnson, C.R. Meyer, T.L. Chenevert, L.W. Turnbull, B.D. Ross, Multi-site clinical evaluation of DW-MRI as a treatment response metric for breast cancer patients undergoing neoadjuvant chemotherapy, PLoS One 10 (3) (2015) e0122151.

[21] X.R. Li, L.Q. Cheng, M. Liu, Y.J. Zhang, J.D. Wang, A.L. Zhang, X. Song, J. Li, Y.Q. Zheng, L. Liu, DW-MRI ADC values can predict treatment response in patients with locally advanced breast cancer undergoing neoadjuvant chemotherapy, Med. Oncol. 29 (2) (2012) 425–431.

[22] U. Sharma, K.K. Danishad, V. Seenu, N.R. Jagannathan, Longitudinal study of the assessment by MRI and diffusion-weighted imaging of tumor response in patients with locally advanced breast cancer undergoing neoadjuvant chemotherapy, NMR Biomed. 22 (1) (2009) 104–113.

[23] R. Bedair, A.N. Priest, A.J. Patterson, M.A. McLean, M.J. Graves, R. Manavaki, A.B. Gill, O. Abeyakoon, J.R. Griffiths, F.J. Gilbert, Assessment of early treatment response to neoadjuvant chemotherapy in breast cancer using non-mono-exponential diffusion models: a feasibility study comparing the baseline and mid-treatment MRI examinations, Europeanradiology 27 (7) (2017) 2726–2736.

[24] S. Kim, L. Decarlo, G.Y. Cho, J.H. Jensen, D.K. Sodickson, L. Moy, S. Formenti, R.J. Schneider, J.D. Goldberg, E.E. Sigmund, Interstitial fluid pressure correlates with intravoxel incoherent motion imaging metrics in a mouse mammary carcinoma model, NMR Biomed. 25 (5) (2012) 787–794.

[25] E.A. Eisenhauer, P. Therasse, J. Bogaerts, L.H. Schwartz, D. Sargent, R. Ford, J. Dancey, S. Arbuck, S. Gwyther, M. Mooney, L. Rubinstein, L. Shankar, L. Dodd, R. Kaplan, D. Lacombe, J. Verweij, New response evaluation criteria in solid tumours: revised RECIST guideline (version 1.1), Eur. J. Cancer 45 (2) (2009) 228–247.

[26] S. Nougaret, H.A. Vargas, Y. Lakhman, R. Sudre, R.K. Do, F. Bibeau, D. Azria, E. Assenat, N. Molinari, M.A. Pierredon, P. Rouanet, B. Guiu, Intravoxel incoherent motion-derived histogram metrics for assessment of response after combined chemotherapy and radiation therapy in rectal cancer: initial experience and comparison between single-Section and volumetric analyses, Radiology 280 (2) (2016) 446–454.

[27] E. Bufi, P. Belli, M. Costantini, A. Cipriani, M. Di Matteo, A. Bonatesta, G. Franceschini, D. Terribile, A. Mule, L. Nardone, L. Bonomo, Role of the apparent diffusion coefficient in the prediction of response to neoadjuvant chemotherapy in patients with locally advanced breast cancer, Clin. Breast Cancer 15 (5) (2015) 370–380.

[28] R. Richard, I. Thomassin, M. Chapellier, A. Scemama, P. de Cremoux, M. Varna, S. Giacchetti, M. Espie, E. de Kerviler, C. de Bazelaire, Diffusion-weighted MRI in pretreatment prediction of response to neoadjuvant chemotherapy in patients with breast cancer, Eur. Radiol. 23 (9) (2013) 2420–2431.

[29] G. Belli, S. Busoni, A. Ciccarone, A. Coniglio, M. Esposito, M. Giannelli, L.N. Mazzoni, L. Nocetti, R. Sghedoni, R. Tarducci, G. Zatelli, R.A. Anoja, G. Belmonte, N. Bertolino, M. Betti, C. Biagini, A. Ciarmatori, F. Cretti, E. Fabbri, L. Fedeli, S. Filice, C.P. Fulcheri, C. Gasperi, P.A. Mangili, S. Mazzocchi, G. Meliado, S. Morzenti, L. Noferini, N. Oberhofer, L. Orsingher, N. Paruccini, G. Principagalli, M. Quattrocchi, A. Rinaldi, D. Scelfo, G.V. Freixas, L. Tenori, I. Zucca, C. Luchinat, C. Gori, G. Gobbi, M.R.I. Italian Association of Physics in Medicine Working Group on, Quality assurance multicenter comparison of different MR scanners for quantitative diffusion-weighted imaging, J. Magn. Reson. Imaging: JMRI 43 (1) (2016) 213–219.

[30] N.P. Jerome, K. Miyazaki, D.J. Collins, M.R. Orton, J.A. d'Arcy, T. Wallace, L. Moreno, A.D. Pearson, L.V. Marshall, F. Carceller, M.O. Leach, S. Zacharoulis, D.M. Koh, Repeatability of derived parameters from histograms following non-Gaussian diffusion modelling of diffusion-weighted imaging in a paediatric oncological cohort, Eur. Radiol. 27 (1) (2017) 345–353.